

# Tailoring tunnel magnetoresistance by ultrathin Cr and Co interlayers: A first-principles investigation of Fe/MgO/Fe junctions

Peter Bose,<sup>1,2</sup> Peter Zahn,<sup>1</sup> Jürgen Henk,<sup>3</sup> and Ingrid Mertig<sup>1,3</sup>

<sup>1</sup>*Martin Luther University Halle-Wittenberg, Institute of Physics, D-06099 Halle (Saale), Germany*

<sup>2</sup>*International Max Planck Research School for Science and Technology  
of Nanostructures, Weinberg 2, D-06120 Halle (Saale), Germany*

<sup>3</sup>*Max Planck Institute of Microstructure Physics, Weinberg 2, D-06120 Halle (Saale), Germany  
(Dated: July 28, 2021)*

We report on systematic ab-initio investigations of Co and Cr interlayers embedded in Fe(001)/MgO/Fe(001) magnetic tunnel junctions, focusing on the changes of the electronic structure and the transport properties with interlayer thickness. The results of spin-dependent ballistic transport calculations reveal options to specifically manipulate the tunnel magnetoresistance ratio. The resistance area products and the tunnel magnetoresistance ratios show a monotonous trend with distinct oscillations as a function of the Cr thickness. These modulations are directly addressed and interpreted by means of magnetic structures in the Cr films and by complex band structure effects. The characteristics for embedded Co interlayers are considerably influenced by interface resonances which are analyzed by the local electronic structure.

PACS numbers: 72.25.Mk, 73.22.-f, 73.40.Gk, 75.47.-m

## I. INTRODUCTION

During the last years magnetoresistive effects — in particular the tunnel magnetoresistance (TMR) effect<sup>1,2</sup> — became increasingly important for the fast developing field of spintronic devices<sup>3,4</sup>. The first industrial applicable TMR contacts have been built using crystalline MgO insulators which are epitaxially grown on as well as coated with iron electrodes<sup>5,6</sup>. Fe/MgO/Fe magnetic tunnel junctions (MTJs) have been extensively investigated to elucidate the mismatch between theoretically predicted<sup>7,8</sup> and the at least one order of magnitude smaller measured<sup>9,10</sup> TMR ratios. It turned out that the disparity can be attributed to differences between idealized (in theory) and real (in experiment) samples. More sophisticated theories which include imperfections, like interface disorder<sup>11–17</sup> or roughness effects<sup>18</sup>, were able to close the gap between experiment and theory and highlight the importance of perfect interfaces.

Although other tunnel junctions, like CoFeB/MgO/CoFeB MTJs with their high TMR ratios<sup>19</sup>, were put into the focus of attention, Fe/MgO/Fe MTJs are still intensely studied. Besides the emerging field of spin-torque effects<sup>20</sup>, research is ongoing in search of other ways to increase the TMR ratio further. Instead of improving the interface quality an alternative means is found in the specific manipulation of the spin-dependent conductances by embedding ultrathin interlayers<sup>21,22</sup>.

The insertion of a single layer-wise antiferromagnetic (LAFM) Cr interlayer results into even-odd oscillations of the TMR ratio as a function of the Cr thickness<sup>23,24</sup>. In this paper we report on a first-principles study of these transport characteristics. We discuss the origin of these modulations with the apparent 2 ML-wavelength as well.

Additionally, an analysis of the electronic transport results for Co interlayers at both Fe/MgO interfaces is presented. These investigations were motivated by previous ab-initio calculations<sup>25</sup> which predicted larger TMR ratios for MgO tunnel junctions with bcc Co(001) leads instead of Fe(001) electrodes. Due to the fact that Co grows epitaxially only up to a few monolayers on bcc substrates, a question arises whether ultrathin Co interlayers could be alternatively used to obtain an enhancement of the TMR ratios in Fe/MgO/Fe MTJs. To answer this question we computed the conductances and TMR ratios for small Co interlayer thicknesses and analyzed the results by means of the electronic structures.

## II. THEORETICAL BACKGROUND

Our computational approach is divided into two steps. Firstly, the electronic structures of the MTJs are calculated from first principles. Secondly, the electronic transport properties are computed, using the potentials obtained in the first step.

The electronic structure is determined self-consistently within the framework of density-functional theory (DFT) using a scalar-relativistic screened Korringa-Kohn-Rostoker (KKR) Green function technique<sup>26,27</sup>. The spherical site potentials were treated in the atomic sphere approximation (ASA) using the local spin density approximation (LSDA) for the exchange-correlation potential<sup>28</sup>. Throughout this work a parameterization following Vosko, Wilk, and Nusair<sup>29</sup> was used.

Since structural information of Fe/MgO/Fe MTJs with embedded ultrathin Cr and Co spacers are not reported so far, we resort to a geometry of planar Fe(001)/MgO/Fe(001) junctions which has been determined experimentally by surface x-ray diffraction

analyses<sup>30,31</sup>. This structure has been used in previous theoretical studies<sup>16,32</sup>. In detail, a super-cell geometry with six MgO layers sandwiched by 20 Fe layers was used to compute self-consistently the atomic potentials. The insertion of  $x$  magnetic interlayers in planar Fe(001)/ $x$ (Cr)/6(MgO)/Fe(001) and Fe(001)/ $x$ (Co)/6(MgO)/ $x$ (Co)/Fe(001) junctions was achieved by replacing  $x$  Fe monolayers (ML) at the Fe/MgO interfaces by  $x$  Cr or Co layers. This procedure implies that Cr and Co atoms occupy the same positions as the replaced Fe atoms; worded differently, the interlayers follow the bcc structure of the Fe(001) leads.

Due to the broken translational invariance in transport direction ( $z$ , i.e. [001]) and the in-plane translational invariance, the eigenstates of the electrodes are labeled by in-plane wave vectors  $\mathbf{k}_{||} = (k_x, k_y)$ . The point group of the two-dimensional lattice is  $4mm$ .

The ballistic conductance  $C$  per unit cell area  $A_{\square}$  is computed for zero bias voltage in terms of transmission probabilities (Landauer-Büttiker approach<sup>33</sup>) at the Fermi energy  $E_F$ ,

$$C = \frac{e^2}{h} \int_{2\text{BZ}} T(\mathbf{k}_{||}, E_F) d\mathbf{k}_{||}. \quad (1)$$

The transmission probability  $T(\mathbf{k}_{||}, E_F)$  is obtained by means of a Green function approach<sup>34</sup>. The integration over the two-dimensional Brillouin zone (2BZ) requires typically about 90 000  $\mathbf{k}_{||}$ . The use of special  $\mathbf{k}_{||}$  points<sup>35</sup> reduces that number to 1/8. The resistance area product

$$RA = \frac{1}{C}, \quad (2)$$

as normalized quantity, is used to compare the theoretical with experimental data.

The optimistic TMR ratio is obtained from the RAs which are computed for the parallel (P) and the anti-parallel (AP) alignment of the two Fe(001) lead magnetizations,

$$\text{TMR} = \frac{RA^{\text{AP}} - RA^{\text{P}}}{RA^{\text{P}}}. \quad (3)$$

For the normalized TMR ratio the denominator is replaced by  $RA^{\text{AP}} + RA^{\text{P}}$ . Since interfaces determine considerably the transport properties, transmittance maps which display  $T(\mathbf{k}_{||}, E_F)$  versus  $\mathbf{k}_{||}$  need to be interpreted by means of the local electronic structure, rather than by the electronic structures of the bulk electrodes. The former is obtained from the layer-resolved Bloch spectral density (SD)

$$N_{al}(E, \mathbf{k}_{||}) = -\frac{1}{\pi} \text{ImTr} G_{al}^+(E, \mathbf{k}_{||}), \quad (4)$$

of atom  $a$  in layer  $l$ .  $G_{al}^+(E, \mathbf{k}_{||})$  is the site-diagonal Green function of that site. The trace involves integration over the ASA sphere and summation over spin-angular quantum numbers.

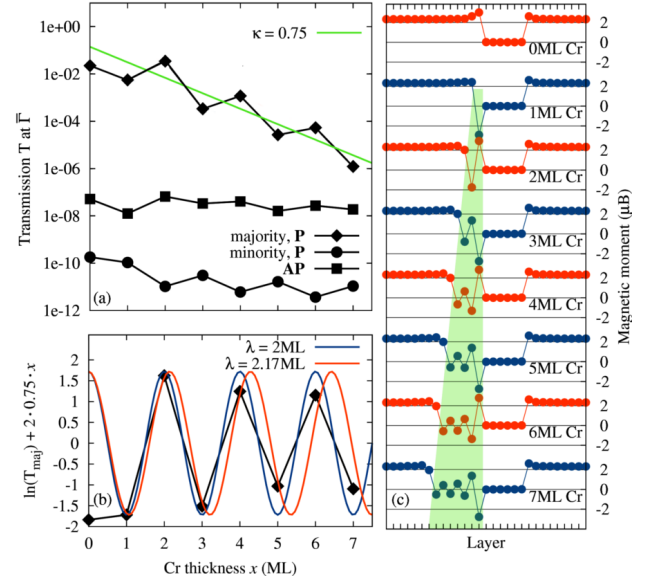


Figure 1: (Color) (a) Dependence of spin-resolved P (majority, minority) and AP transmissions on a logarithmic scale versus Cr thickness  $x$  for Bloch states at  $\mathbf{k}_{||} = 0$  in Fe(001)/ $x$ (Cr)/6(MgO)/Fe(001) MTJs,  $x = 0, \dots, 7$ . The green line is a fitted exponential to the majority transmission. The deviation of the majority transmission from this fit is shown in panel (b). These data are fitted by cosine functions (fixed at  $x = 1$ ) with 2 ML (blue) and 2.17 ML (red) periods. (c) Magnetic profiles of MTJs with Cr layer thicknesses  $x = 0, \dots, 7$  ML. The green area highlights the magnetic moments of the Cr layers.

### III. RESULTS

#### A. Cr interlayer in Fe(001)/MgO/Fe(001)

In the following we present results of the thickness dependence of both the conductances and the TMR ratios for ultra-thin Cr interlayers which are embedded at a single interface in Fe(001)/ $x$ (Cr)/6(MgO)/Fe(001) MTJs. The Cr thickness  $d_{\text{Cr}}$  is varied in steps of monolayers (ML),  $x = 0, \dots, 7$  with  $d_{\text{Cr},1\text{ ML}} = 2.35 \text{ \AA}$ ,  $d_{\text{Cr},2\text{ ML}} = 4.04 \text{ \AA}$  and  $d_{\text{Cr},x\text{ ML}} = d_{\text{Cr},2\text{ ML}} + x \cdot 1.69 \text{ \AA}$ .

We start with the tunneling behavior of Bloch states at  $\bar{\Gamma}$  ( $\mathbf{k}_{||} = 0$ ). The associated transmission probabilities for  $x = 0, \dots, 7$  are plotted in Fig. 1a. Both the minority spin contribution for P and the AP contribution stay almost constant, whereas the majority spin contribution of P decays exponentially with an oscillatory modulation. Its decay rate is estimated by an exponential fit,  $\exp(-2\kappa x)$  with  $\kappa = 0.75$  (green line in Fig. 1a).

It turns out that an oscillatory modulation of  $T_{\text{maj}}^{\text{P}}$  shows up for all  $\mathbf{k}_{||}$  within the 2BZ. These oscillations are also present in the conductance  $C$  which is an integral over the transmission probabilities, eq. (1); hence, there is no destructive interference which would lead to (complete) cancellation. Thus, it is essential to eluci-

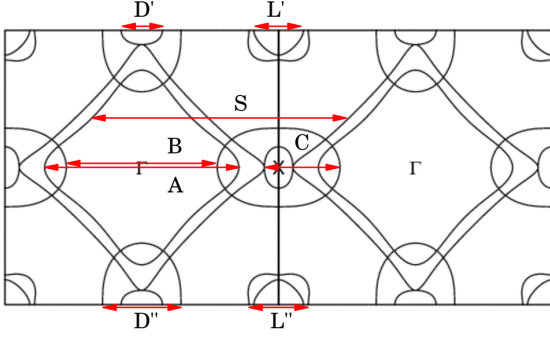


Figure 2: (Color online) Fermi surface cross sections in the (100) plane of commensurate AFM Cr (c-afm). The nesting vectors along [001] (arrows) are shown in an extended zone scheme and are listed in Table I.

Table I: Nesting vectors of commensurate AFM (c-afm) Cr along [001], as given in Fig. 2, are characterized by their oscillation periods (in ML).

c-afm	L'	L''	S	A	B	C	D'	D''
$\lambda[\text{ML}]$	11.03	9.21	2.12	2.82	3.62	7.21	13.26	6.96

date the underlying mechanism of these oscillations. To strengthen the discussion we focus in the following on the transmissions at  $\bar{\Gamma}$ .

The oscillation period can be estimated by fitting cosine functions to the deviation of  $T_{\text{maj}}^P(\mathbf{k}_{\parallel} = 0)$  from the averaged exponential decay (black diamonds in Fig. 1b). The fit with a period of 2 ML (blue) reproduces only the peak positions but deviates significantly in amplitude. A second fit, with 2.17 ML period (red), hits the data best.

The 2 ML oscillation can be explained by the local magnetic structure of the layer-wise antiferromagnetic (LAFM) Cr interlayers (Fig. 1c). The magnetic moments of the Cr layers at the Cr/MgO interface is sizably enhanced due to the nonmagnetic MgO film. As a consequence of these partially uncompensated magnetic moments, the Cr interface layers act as spin filters for the tunnel currents. Hence, the latter are increased (decreased) if the magnetic moments within the Cr interface layers are parallel (anti-parallel) to the magnetization of the opposite Fe electrode. Due to the LAFM growth of the Cr interlayer the tunnel current characteristics should exhibit signatures of 2 ML oscillations. The maxima of these oscillations should arise for P (AP) magnetic configurations of the Fe leads at even (odd) multiples of the Cr interlayer thickness  $x$ . This behaviour was already found for LAFM Mn interlayers in Fe(001)/ $x$ (Mn)/Vac/Fe(001) MTJs<sup>36</sup>. However, the mismatch in Fig. 1b appears like an undersampling which cannot be satisfactorily explained by means of the spin filter effect. The better match of the other oscillation period with 2.17 ML points to another effect which additionally influences the electronic transport.

There are two possible mechanisms that may explain

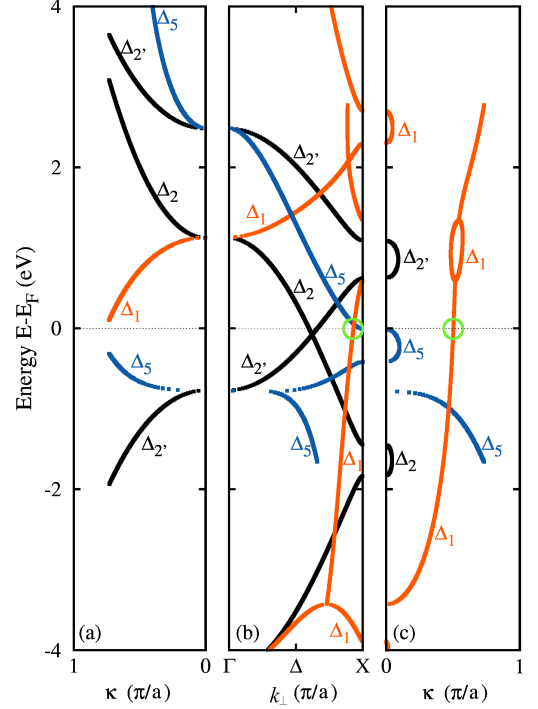


Figure 3: (Color) Complex bandstructure of bulk bcc Cr in the commensurate AFM (c-afm) phase along [001] for  $\mathbf{k}_{\parallel} = 0$ . The real part of  $k_{\perp}$  and the exponential decay rate  $\kappa$  (imaginary part of  $k_{\perp}$ ) are shown in panels (b) and (a, c), respectively. The color code of the bands indicates the irreducible representations of the point group  $4mm$  of the associated Bloch states. The green circles at the Fermi energy mark the complex  $\Delta_1$ -band of second kind, to  $k_{\perp} = (0.922, 0.503)\pi/a$ , which governs the transmission of majority electrons at  $\bar{\Gamma}$  (cf. Fig. 1a).

other wavelengths than the 2 ML. Firstly, one could think of spin-density waves within the Cr interlayers. Spin-density waves are found for Cr bulk systems<sup>37</sup> and are related to nesting vectors of the Fermi surface. Nesting vectors that come into question are shown in Fig. 2 for a cross section of the Fermi surface in the (100) plane. The corresponding wavelengths of these vectors along the [001] direction (i.e. in transport and growth direction) are given in Table I. The only vector that exhibits a wavelength which is comparable to that of the transmission (2.17 ML) is S, with an oscillation period of 2.12 ML. However, since we are interested in the oscillatory onset at  $\mathbf{k}_{\parallel} = 0$ , the vector S cannot explain our findings because it is offset from  $\bar{\Gamma}$ .

The oscillatory exponential decay of  $T_{\text{maj}}^P(\mathbf{k}_{\parallel} = 0)$  is explained most promisingly in terms of the complex bandstructure<sup>38</sup> of the Cr interlayers. Since a (continuous) dispersion relation is not defined for thin films, due to lack of translational invariance, we refer to the complex bandstructure of bulk Cr along [001]. The latter is decomposed with respect to the irreducible representa-

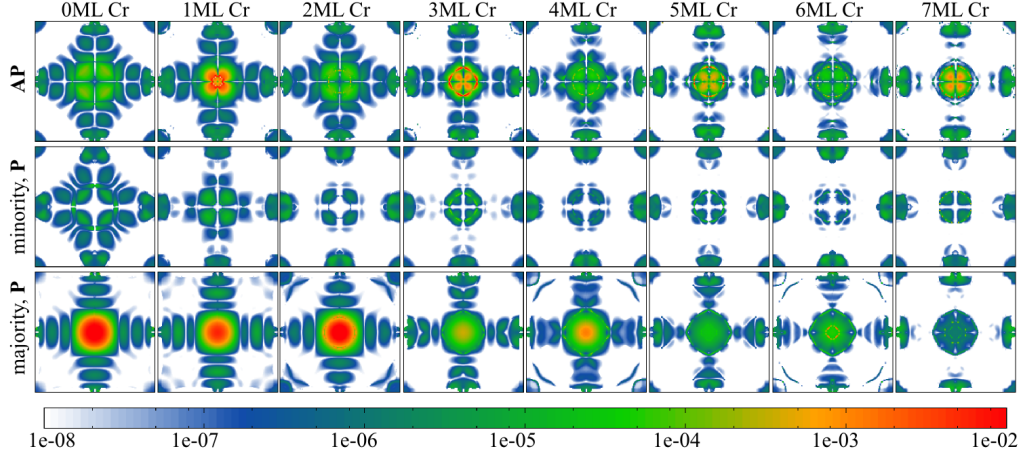


Figure 4: (Color online) Majority (P, bottom row), minority (P, middle row) and AP (top row) transmission  $T(\mathbf{k}_{||}, E_F)$  within two-dimensional Brillouin zones for Fe(001)/ $x$ (Cr)/6(MgO)/Fe(001) MTJs with Cr layer thicknesses of  $x = 0, \dots, 7$  ML (from left to right). The two-dimensional Brillouin zones cover the range between  $-\pi/a$  and  $\pi/a$ .

tions of the point group  $4mm$  ( $\Delta_1$ ,  $\Delta_5$ ,  $\Delta_2$  and  $\Delta_2'$ ) of the associated Bloch states (Fig. 3).

A complex band structure of a periodic system is the conventional band structure extended to Bloch vectors  $(\mathbf{k}_{||}, k_{\perp})$  with complex wave numbers  $k_{\perp}$ . The associated bands can be cast into four categories<sup>39</sup>: (i) *real bands* which correspond to the conventional band structure and have  $\text{Im}k_{\perp} = 0$ ; (ii) *imaginary bands of the first kind* have  $\text{Re}k_{\perp} = 0$  and  $\text{Im}k_{\perp} \neq 0$ ; (iii) *imaginary bands of the second kind* with  $\text{Re}k_{\perp} = \pi/a$  and  $\text{Im}k_{\perp} \neq 0$ ; and (iv) *complex bands* with  $\text{Re}k_{\perp} \neq 0$ ,  $\text{Re}k_{\perp} \neq \pi/a$  and  $\text{Im}k_{\perp} \neq 0$ .

The imaginary part of  $k_{\perp}$  is denoted as  $\kappa$  and represents a measure for the decay rate of evanescent Bloch states<sup>43</sup>. At the Fermi energy, a complex band of the second kind shows up at  $k_{\perp} = (0.922, 0.503)\pi/a$  (circles in Fig. 3). The corresponding decay rate of  $\kappa = 0.78/\text{ML}$  matches well the estimated exponential decay of the majority transmission ( $\kappa = 0.75/\text{ML}$ , Fig. 1a). Due to the nonvanishing real part the exponential decay exhibits an oscillatory envelope with a wavelength  $\lambda = \pi/\text{Re}[k_{\perp}] \approx 2.17\text{ML}$  which agrees well with the fit in Fig. 1b. We conclude therefore that the thickness dependence of the transmission for the majority states at the  $\bar{\Gamma}$  point is very likely governed by this  $\Delta_1$  state, provided the electronic structure of ultra-thin Cr films is well described by that of bulk Cr.

Transmission maps display the spin-resolved transmission for P and AP versus  $\mathbf{k}_{||}$  for each Cr thickness  $x$  (Fig. 4). As observed for  $T_{\text{maj}}^P(\mathbf{k}_{||} = 0)$  one finds within the majority transmission maps a clearly visible modulation of  $T_{\text{maj}}^P(\mathbf{k}_{||})$  for  $\mathbf{k}_{||}$ -points in the center regions with maxima (minima) at even (odd) multiples of  $x$ . It is reasonable to assume that the oscillations of these transmissions are caused by the same bandstructure effect as it was discussed for  $T_{\text{maj}}^P$  at  $\bar{\Gamma}$ . Furthermore, the majority  $RA$  products in Fig. 5 exhibit even-odd oscillations

as well, indicating constructive superposition of the oscillations of the individual  $T_{\text{maj}}^P(\mathbf{k}_{||})$ .

Although the cloverleaf-like structures within the mi-

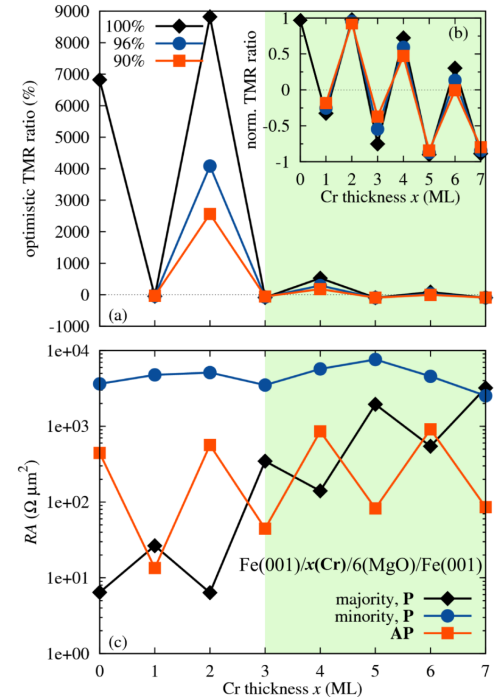


Figure 5: (Color online) Cr thickness dependence of (a) optimistic and (b) normalized TMR ratios in Fe(001)/ $x$ (Cr)/6(MgO)/Fe(001) MTJs. Since variations of the Cr layer thickness cannot be ruled out in experiment, a model with resistors in parallel connection is assumed to mimic Cr-thickness fluctuations (line styles indicate the weight  $w$ ; see text). (c) Resistance area product  $RA$  for parallel magnetic (P: majority, minority) and anti-parallel magnetic configurations (AP), shown on a logarithmic scale.



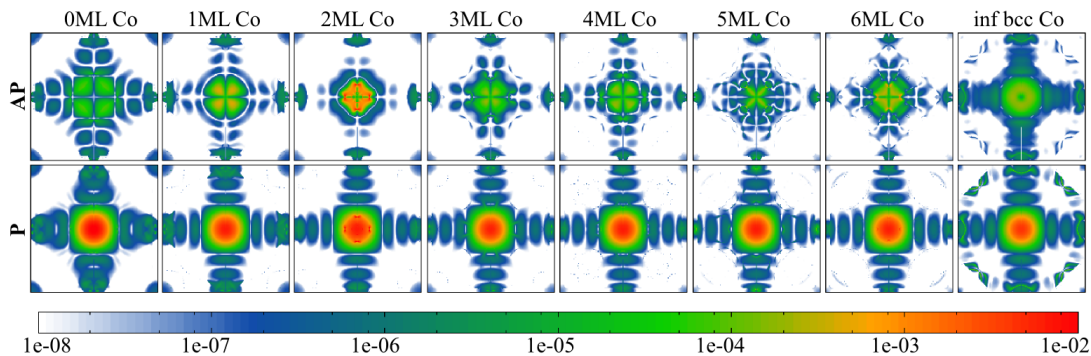


Figure 6: (Color online) Transmission  $T(\mathbf{k}_{\parallel}, E_F)$  for the P (bottom row) and AP (top row) magnetic configuration within two-dimensional Brillouin zones for  $\text{Fe}(001)/x(\text{Co})/6(\text{MgO})/x(\text{Co})/\text{Fe}(001)$  MTJs,  $x = 0, \dots, 6$  ML (from left to the right). The panels on the right hand side are for  $\text{Co}(001)/6(\text{MgO})/\text{Co}(001)$  MTJs with infinite bcc Co leads. The Brillouin zones cover the range between  $-\pi/a$  and  $\pi/a$ .

nority transmission maps in Fig. 4 exhibit slight variations which are in anti-phase to the majority transmission modulations, the corresponding  $RA$  products in Fig. 5 reveal no signatures of such an even-odd characteristic. The weak thickness dependence can be understood with help of the complex bandstructure in Fig. 3. From first-principles investigations on  $\text{Fe}/\text{MgO}/\text{Fe}$  it is known<sup>40,41</sup> that  $\Delta_5$  states are the main carrier within the minority transport channel. Due to the  $\Delta_5$  *real band* at the Fermi energy it is very likely that these Bloch states just propagate undamped through the Cr interlayer. The minority  $RA$  is therefore marginally affected by the Cr spacer and gives contributions which are similar to those of  $\text{Fe}/\text{MgO}/\text{Fe}$  MTJs.

In contrast to the above finding, the pronounced modulations within the AP transmission maps in Fig. 4 — with maxima (minima) at odd (even)  $x$  — lead to an even-odd oscillation of the corresponding  $RA$ . Due to the spin-filter effect of the Cr interface layer  $RA^{\text{AP}}$  is in anti-phase to  $RA^{\text{P}}_{\text{maj}}$ . This behavior results in TMR ratios which exhibit 2ML oscillations with periodic changes of the sign. The amplitudes of the TMR ratios, are with about 7000 % and 9000 % at  $x = 0$  ML and 2 ML, considerably larger than for the other thicknesses, with values between about  $-100$  % and  $+100$  %. This even-odd oscillation of the TMR ratio as a function of the Cr thickness has been observed experimentally<sup>24</sup> but with a phase shift of 1 ML. In more recent experiments<sup>44</sup> it has been found that this phase shift depends on whether the Cr interlayer is grown after or before growth of the MgO barrier. However, a large maximum of the TMR ratio for small Cr thicknesses does not show up in both growth conditions. Instead, an exponential decay of the optimistic TMR ratio for increasing  $x$  is reported<sup>24</sup>. Since variations of the Cr layer thickness cannot be ruled out in experiment, we assume a model with resistors in parallel connection to mimic Cr-thickness fluctuations. The resistance of the mean thickness  $x$  is weighted by  $w$ , the contributions from  $x-1$  and  $x+1$  are weighted by  $(100\% - w)/2$ , respectively. With already large central weights of  $w = 96\%$  and  $w = 90\%$

this model is able to reproduce the principal experimental TMR characteristics<sup>24</sup>. For a detailed analysis of the effect of structural imperfections, however, one has to rely on more sophisticated computational approaches, like the coherent potential approximation or a supercell method.

## B. $\text{Fe}(001)/x(\text{Co})/6(\text{MgO})/x(\text{Co})/\text{Fe}(001)$

In this section we discuss the effects of Co interlayers embedded into  $\text{Fe}(001)/\text{MgO}/\text{Fe}(001)$  MTJs on the electronic transport. With respect to previous theoretical investigations of MgO barriers with bcc Co leads<sup>25</sup> we specifically studied the thickness dependence of ultrathin Co interlayers which are inserted at *both*  $\text{Fe}/\text{MgO}$  interfaces. Since Co grows epitaxially only up to few ML on a bcc substrate, the Co thicknesses  $d_{\text{Co}}$  are restricted to  $x \leq 6$  ML. The monolayer separations are taken identical to the case of Cr interlayers. Substituting all Fe atoms with Co atoms the effect of semi-infinite bcc Co leads is studied in addition.

First, we recall previously reported conductances and TMR ratios in MTJs with equal thickness variations of both Co interlayers<sup>42</sup>. The corresponding  $\mathbf{k}_{\parallel}$ -resolved transmissions versus  $x$  are shown in Fig. 6 for both magnetic configurations (P, AP). The shapes of the transmission maps for P configuration (bottom row) are — beside the case of the semi-infinite Co leads — very similar. In contrast to this weak dependence, one observes a rise and a decline of the transmission probabilities in the central regions of the Brillouin zones for the AP configuration for small  $x$  (top row). The maximum shows up at  $x = 2$  ML. Based on these observations it is reasonable to expect a relatively constant behavior of the P conductance and a maximum at  $x = 2$  ML for the AP conductance.

The elsewhere published conductances and TMR ratios<sup>42</sup> are inserted into Fig. 7 as red boxes. In accordance with the findings for bcc Co leads<sup>25</sup>, we identify specific Co thicknesses ( $x = 3$  ML and 5 ML) that ex-

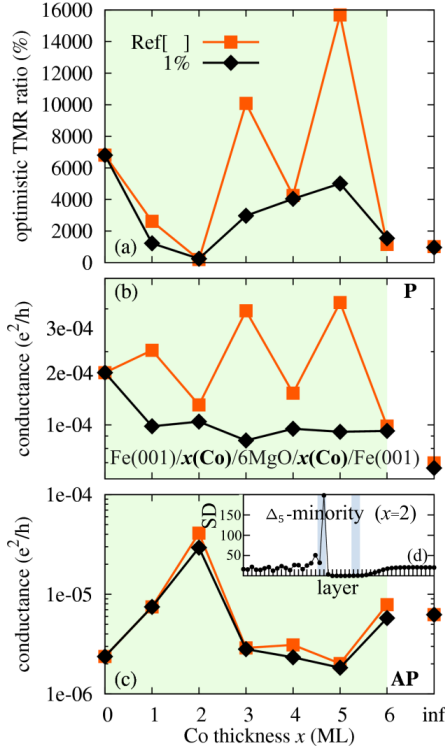


Figure 7: (Color) Co thickness dependence of (a) optimistic TMR ratio, P (b), and AP (c) conductances in symmetric Fe(001)/x(Co)/6(MgO)/x(Co)/Fe(001) MTJs. Red squares, taken from Ref. 42, are for data which exhibit hotspots in the transmission probabilities  $T(\mathbf{k}_{||}, E_F)$ . The black symbols show the data with these hot spots being removed (see text). Panel (d) displays the layer-resolved spectral density (in states/Hartree) of a  $\Delta_5$ -minority interface resonance with  $\mathbf{k}_{||} = (0.095, 0.008)\pi/a$ . The blue areas mark the position of the 2 ML thick Co interlayers within the MTJ.

hibit larger TMR values than those obtained for pure Fe/MgO/Fe junctions. In particular, the TMR ratio follows the even-odd type characteristic which shows up for the conductance  $C^P$ . But, this behavior of  $C^P$  does not reflect the weak thickness dependence as expected from the transmission probabilities (Fig. 6). It turned out that this even-odd change is considerably affected by single interface resonances whose transmission probabilities contribute with up to 70 % to the conductance. These hot spots within the transmission maps occur preferably in ideal, symmetric MTJs at zero bias voltage<sup>21</sup>. They are strongly diminished by breaking the symmetry, for instance by means of a tiny bias voltage or structural imperfections of the sample. A bias voltage of 0.02 V is sufficient to destroy the resonant states and to reduce the corresponding transmission probabilities by several orders of magnitude.

The total number of hot spots in each transmission map of Fig. 6 is less than 10. Instead of removing the resonances by a small bias voltage, the transmissions of these states are identified and neglected. These filtered data are shown as black diamonds in Fig. 7. The effect

of the resonances shows up mainly for  $C^P$ . For the latter one obtains, after an initial decrease of about 50 % from  $x = 0$  ML to 1 ML, the expected nearly constant behavior.

The filtered AP conductances agree well with unfiltered ones, in particular the maximum at  $x = 2$  ML. Inspecting the corresponding transmission map (Fig. 6), this maximum is attributed to enhanced transmissions in the center region of the 2BZ which are caused by  $\Delta_5$ -minority interface resonances within the Co interface layer (Fig. 7d). In contrast to the transmission resonances (hot spots), these transmissions are unaffected by small bias voltages.

Since the thickness dependence of  $C^P$  is weakened by the filter procedure, that of the TMR ratio is as well. In particular, the maxima at  $x = 3$  ML and 5 ML do not show up. The minimum of approximately 200% at  $x = 2$  ML is, however, still present; it is explained by the increase of  $C^{AP}$  — up to a value comparable with  $C^P$  — due to the  $\Delta_5$ -minority interface resonances. For increasing  $x$  the TMR ratio increases monotonously up to a maximum at  $x = 5$  ML, with 4600 % considerably smaller than the 7000 % obtained for pure Fe/MgO/Fe MTJs.

We note in passing that the enhanced TMR ratio in MTJs with semi-infinite bcc Co leads, reported in

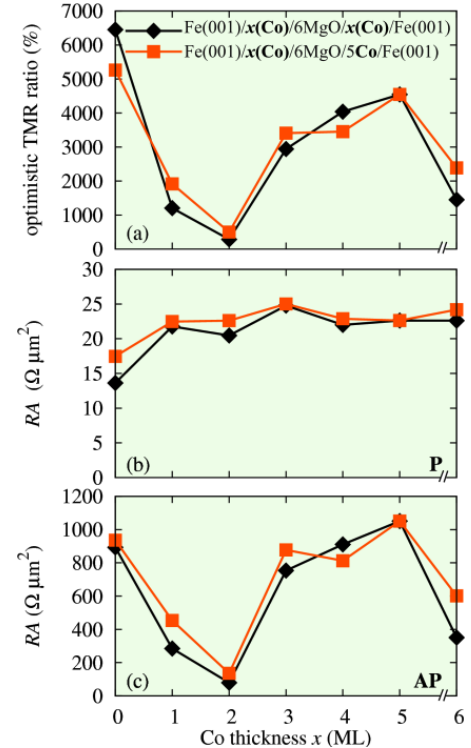


Figure 8: (Color) Optimistic TMR ratios (a) and resistance-area products  $RA$  for P (b) and AP (c) of symmetric (black) and asymmetric (red) Fe(001)/x(Co)/6(MgO)/y(Co)/Fe(001) MTJs. Hot spots were filtered out (see e.g. Fig. 7).

Ref. 25, are not reproduced. Previous investigations of Fe/MgO/Fe systems have shown that conductances depend strongly on details of the calculations, in particular on the atomic positions in the interface region. Thus, one is lead to attribute the above mentioned discrepancy to computational details.

Since increased TMR ratios are not obtained by symmetric MTJs, we studied the effect of asymmetric MTJs, with one interlayer thickness fixed to 5 ML, in addition. The fixed thickness of 5 ML is chosen with respect to the largest TMR ratio in symmetric MTJs (Fig. 7). Both the  $RA$  products and the TMR ratios of the asymmetric junctions do not differ significantly from those of the symmetric junctions (Fig. 8). For both kinds of MTJs, the TMR ratio follows the characteristics of  $RA^{\text{AP}}$  because  $RA^{\text{P}}$  is almost constant. The presence of the minimum at  $x = 2$  ML additionally substantiates that the  $\Delta_5$ -minority interface resonances, which cause the drop of  $RA^{\text{AP}}$ , are marginally affected by symmetry breaking of an ideal MTJ.

#### IV. CONCLUSION

In summary, the computed conductances and TMR ratios exhibit the oscillatory decays for thickness variations of ultrathin Cr interlayers, which have been found in experiment. The analysis of the associated transmission probabilities reveals that the tunneling of Bloch states is affected by the interplay of two mechanisms. On the

one hand a spin-filter effect which is induced by the enhanced magnetic moments of the Cr interface layers and on the other hand the presence of complex bands which are formed within the Cr interlayers. The oscillations are therefore mixtures of 2 ML oscillations of magnetic origin and superpositions of the individual modulations of the tunneling Bloch states, which can be traced back to the corresponding complex wave vectors. Our results further indicate that spin-density waves are of minor importance for understanding of electronic transport through Fe/MgO/Fe MTJs with ultrathin Cr interlayers.

The embedding of Co interlayers at both interfaces does not lead to an increase of the TMR ratios with respect to Fe/MgO/Fe MTJs. Please note that the reference values for  $x = 0$  (i.e. no Co interlayer) have been calculated under the assumption of ideal interface structures and are therefore probably considerably overestimated. Thus, we suggest to include the effects of imperfect interfaces, which are unavoidable in real samples, in a future investigation.

#### Acknowledgments

Helpful discussions with S. Yuasa, R. Matsumoto, and N. F. Hinsche are gratefully acknowledged. This work is supported by the Sonderforschungsbereich 762, Functionality of Oxidic Interfaces. P. B. is supported by the International Max Planck Research School for Science and Technology of Nanostructures.

- 
- <sup>1</sup> M. Julliere, Physics Letters A **54**, 225 (1975), ISSN 0375-9601.
  - <sup>2</sup> J. S. Moodera, L. R. Kinder, T. M. Wong, and R. Meservey, Physical Review Letter **74**, 3273 (1995).
  - <sup>3</sup> I. Žutić, J. Fabian, and S. Das Sarma, Reviews of Modern Physics **76**, 323 (2004).
  - <sup>4</sup> S. A. Wolf, A. Y. Chtchelkanova, and D. M. Treger, IBM J. Res. Dev. **50**, 101 (2006), ISSN 0018-8646.
  - <sup>5</sup> W. J. Gallagher and S. S. P. Parkin, IBM J. Res. Dev. **50**, 3 (2006).
  - <sup>6</sup> S. Yuasa and D. D. Djayaprawira, Journal of Physics D: Applied Physics **40**, R337 (2007).
  - <sup>7</sup> W. H. Butler, X.-G. Zhang, T. C. Schulthess, and J. M. MacLaren, Physical Review B **63**, 054416 (2001).
  - <sup>8</sup> J. Mathon and A. Umerski, Phys. Rev. B **63**, 220403 (2001).
  - <sup>9</sup> S. Yuasa, T. Nagahama, A. Fukushima, Y. Suzuki, and K. Ando, Nature Materials **3**, 868 (2004).
  - <sup>10</sup> S. S. P. Parkin, C. Kaiser, A. Panchula, P. M. Rice, B. Hughes, M. Samant, and S.-H. Yang, Nat Mater **3**, 862 (2004), ISSN 1476-1122.
  - <sup>11</sup> X.-G. Zhang, W. H. Butler, and A. Bandyopadhyay, Physical Review B **68**, 092402 (2003).
  - <sup>12</sup> J. Mathon and A. Umerski, Physical Review B **74**, 140404 (2006).
  - <sup>13</sup> H. Itoh, J. Ozeki, and J. Inoue, Journal of Magnetism and Magnetic Materials **303**, e205 (2006).
  - <sup>14</sup> D. Waldron, V. Timoshevskii, Y. Hu, K. Xia, and H. Guo, Physical Review Letters **97**, 226802 (2006).
  - <sup>15</sup> C. Heiliger, P. Zahn, and I. Mertig, Journal of Magnetism and Magnetic Materials **316**, 478 (2007).
  - <sup>16</sup> P. Bose, A. Ernst, I. Mertig, and J. Henk, Physical Review B **78**, 092403 (2008).
  - <sup>17</sup> F. Bonell, S. Andrieu, A. M. Bataille, C. Tiusan, and G. Lengaigne, Physical Review B **79**, 224405 (2009).
  - <sup>18</sup> P. X. Xu, V. M. Karpan, K. Xia, M. Zwierzycki, I. Marushchenko, and P. J. Kelly, Phys. Rev. B **73**, 180402 (2006).
  - <sup>19</sup> S. Ikeda, J. Hayakawa, Y. Ashizawa, Y. M. Lee, K. Miura, H. Hasegawa, M. Tsunoda, F. Matsukura, and H. Ohno, Applied Physics Letters **93**, 082508 (2008).
  - <sup>20</sup> R. Matsumoto, A. Fukushima, K. Yakushiji, S. Yakata, T. Nagahama, H. Kubota, T. Katayama, Y. Suzuki, K. Ando, S. Yuasa, et al., Phys. Rev. B **80**, 174405 (2009).
  - <sup>21</sup> K. D. Belashchenko, J. Velez, and E. Y. Tsybal, Physical Review B **72**, 140404 (2005).
  - <sup>22</sup> F. Greullet, C. Tiusan, F. Montaigne, M. Hehn, D. Halley, O. Bengone, M. Bowen, and W. Weber, Phys. Rev. Lett. **99**, 187202 (pages 4) (2007).
  - <sup>23</sup> T. Nagahama, S. Yuasa, E. Tamura, and Y. Suzuki, Physical Review Letters **95**, 086602 (2005).
  - <sup>24</sup> R. Matsumoto, A. Fukushima, K. Yakushiji, S. Nishioka, T. Nagahama, T. Katayama, Y. Suzuki, K. Ando, and S. Yuasa, Physical Review B **79**, 174436 (2009).

- <sup>25</sup> X.-G. Zhang and W. H. Butler, *Physical Review B* **70** (2004).
- <sup>26</sup> R. Zeller, P. H. Dederichs, B. Újfalussy, L. Szunyogh, and P. Weinberger, *Physical Review B* **52**, 8807 (1995).
- <sup>27</sup> N. Papanikolaou, R. Zeller, and P. H. Dederichs, *J. Phys.: Condens. Matter* **14**, 2799 (2002).
- <sup>28</sup> W. Kohn and L. J. Sham, *Physical Review* **140**, A1133 (1965).
- <sup>29</sup> S. H. Vosko, L. Wilk, and M. Nusair, *Canadian Journal of Physics* **59**, 1200 (1980).
- <sup>30</sup> H. L. Meyerheim, R. Popescu, N. Jedrecy, M. Vedula, M. Sauvage-Simkin, R. Pinchaux, B. Heinrich, and J. Kirschner, *Physical Review B* **65**, 144433 (2002).
- <sup>31</sup> C. Tusche, H. L. Meyerheim, N. Jedrecy, G. Renaud, A. Ernst, J. Henk, P. Bruno, and J. Kirschner, *Physical Review Letters* **95**, 176101 (2005).
- <sup>32</sup> C. Heiliger, P. Zahn, B. Y. Yavorsky, and I. Mertig, *Physical Review B* **72**, 180406 (2005).
- <sup>33</sup> Y. Imry and R. Landauer, *Reviews of Modern Physics* **71**, S306 (1999).
- <sup>34</sup> J. Henk, A. Ernst, K. K. Saha, and P. Bruno, *Journal of Physics: Condensed Matter* **18**, 2601 (2006).
- <sup>35</sup> R. A. Evarestov and V. P. Smirnov, *physica status solidi (b)* **119**, 9 (1983).
- <sup>36</sup> P. Bose, I. Mertig, and J. Henk, *Physical Review B* **75**, 100402 (2007).
- <sup>37</sup> E. Fawcett, *Review of Modern Physics* **60**, 209 (1988).
- <sup>38</sup> V. Heine, *Physical Review* **138**, A1689 (1965).
- <sup>39</sup> Y.-C. Chang, *Physical Review B* **25**, 605 (1982).
- <sup>40</sup> C. Heiliger, P. Zahn, and I. Mertig, *Materials Today* **9**, 46 (2006).
- <sup>41</sup> W. H. Butler, *Science and Technology of Advanced Materials* **9**, 014106 (2008).
- <sup>42</sup> P. Bose, P. Zahn, J. Henk, and I. Mertig, *Novel Materials and Devices for Spintronics* **1183**, FF07 (2009).
- <sup>43</sup> Since  $k_{\perp}$  is commonly defined in units of  $\pi/a$  and  $a$  corresponds to an interlayer distance of 2 ML, a factor of  $\pi/2$  has to be incorporated to obtain it in units of  $1/\text{ML}$ .
- <sup>44</sup> R. Matsumoto and S. Yuasa, private communication.